We are IntechOpen, the world's leading publisher of Open Access books Built by scientists, for scientists

4,800
Open access books available

122,000
International authors and editors

135M
Downloads

Our authors are among the

154
Countries delivered to

TOP 1%
most cited scientists

12.2%
Contributors from top 500 universities

WEB OF SCIENCE™

Selection of our books indexed in the Book Citation Index in Web of Science™ Core Collection (BKCI)

Interested in publishing with us?
Contact book.department@intechopen.com

Numbers displayed above are based on latest data collected.
For more information visit www.intechopen.com

7

Frequency Conversion based on Three-Wave Parametric Solitons

Fabio Baronio[1], Matteo Conforti[1], Costantino De Angelis[1], Antonio Degasperis[2], Sara Lombardo[3,4] and Stefan Wabnitz[1]
[1]*CNISM, Universitá degli Studi di Brescia,*
[2]*Universitá di Roma La Sapienza,*
[3]*Vrije Universiteit,*
[4]*Manchester University,*
[1,2]*Italy*
[3]*The Netherland*
[4]*England*

1. Introduction

Parametric three-wave mixing in quadratic nonlinear crystals provides a versatile means of achieving widely tunable frequency conversion of laser light, thus permitting a substantial extension of the wavelength coverage of laser sources across broad wavelength regions. For mode-locked lasers, the effective parametric interaction length among short pulses at different wavelengths is limited by crystal dispersion, which leads to group velocity walk-off. Nevertheless, as well known since the 1970s, the frequency conversion of short pulses may be significantly enhanced by means of the optical soliton concept (Zakharov & Manakov, 1973). Indeed, the collision of two soliton input pulses at different frequencies, with proper durations and peak powers, leads to a time compressed pulse at the sum-frequency (Ibragimov & Struthers, 1996). However such pulse is unstable, since it rapidly decays into two, time-shifted replicas of the input pulses. On the other hand, two resonant bright pulses and a kink (or phase jump across a CW background) pulse may propagate locked together as an optical simulton, in spite of their different linear group velocities, owing to their nonlinear mutual trapping (Nozaki & Taniuti, 1973; Degasperis et al., 2006).
In this chapter we present at first a self-contained derivation of the three-wave equations in dispersive and quadratic nonlinear crystals. We outline the generality as well as the limitations to the application of the basic three-wave parametric interaction equations, in which intra-pulse chromatic dispersion is neglected. Next we review a recently discovered class of exact simulton solutions of the parametric three-wave interaction (Degasperis et al., 2006; Conforti et al., 2006; Degasperis et al., 2007), which have as potential applications the stable sum and frequency difference generation of short optical pulses and pulse trains. These nonlinear waves are characterised by the property that the group velocity of the two bright pulses and the kink may be controlled by varying the input energy of the wave-packets, or the relative energy distribution among the three waves (Degasperis et al., 2006). It is particularly significant that the common velocity and the relative energy distribution of these mutually trapped pulses may gradually evolve upon propagation through the crystal

Source: Advances in Lasers and Electro Optics, Book edited by: Nelson Costa and Adolfo Cartaxo,
ISBN 978-953-307-088-9, pp. 838, April 2010, INTECH, Croatia, downloaded from SCIYO.COM

(Conforti et al., 2007). Such unique feature may enable one to achieve a stable frequency conversion of short optical pulses, as well as a continuous control of their frequency conversion efficiency by adjusting the input intensity of a continuous wave background wave (Conforti et al., 2007). In addition, the control of the CW power level also permits the highly efficient generation of a frequency converted train of short optical pulses, which represent a time-periodic copy at a different optical frequency of the input short signal pulse (Baronio et al., 2008). We provide simple analytical relations between the time duration, amplitude and repetition rate of the generated pulse sequence, and the parameters of the input short pulse and CW. Finally, we describe the practical conditions for the experimental observation of the above described pulse shaping, generation and speed control effects via parametric three wave mixing in commonly available quadratic nonlinear crystals. In particular, a simple and easily achievable condition must be respected for the linear group velocities of the three interacting waves, namely that the group velocity of the sum-frequency wave must be intermediate between the group velocities of the two fundamental waves.

2. Equations

The resonant interaction of three waves (TWI) is an important process which appears in various contexts of physics, such as fluid dynamics and optics. It describes the mixing of three quasi–monochromatic waves whose wave numbers $\vec{k}_1, \vec{k}_2, \vec{k}_3$ and frequencies ω_1, ω_2, ω_3 satisfy the resonant conditions

$$\vec{k}_1 + \vec{k}_2 = \vec{k}_3 \ , \ \omega_1 + \omega_2 = \omega_3 \tag{1}$$

in weakly nonlinear and dispersive media. In optics this resonant interaction may occur in any nonlinear medium where nonlinear effects are small and can be considered as a perturbation of the linear wave propagation, the lowest-order nonlinearity is quadratic in the field amplitudes and the dispersion relation $\omega(\vec{k})$ allows for the special choice of the wave numbers $\vec{k}_\alpha$, α = 1, 2, 3, such that the phase matching (or resonance) condition (1) is satisfied, where $\omega_\alpha = \omega(\vec{k}_\alpha)$. The proper description of the resonant interaction is provided by a relatively simple model which can be derived from Maxwell equations in a dielectric with quadratic nonlinear susceptibility $\chi^{(2)}$. Here below we first sketch the way to obtain the system of three coupled equations which model the resonant interaction, and then we discuss some of its properties together with special solutions of applicative interest.

If $\vec{P}(\vec{r},t)$ is the dielectric polarization vector field induced by the electromagnetic wave, the charge and current densities in the medium are (hereafter a subscripted variable stands for partial differentiation with respect to that variable, and a dot between two vectors indicates their scalar product)

$$\rho = -\vec{\nabla}_r \cdot \vec{P} \ , \ \vec{J} = \vec{P}_t \ , \tag{2}$$

so that Maxwell's equations reduce in a standard way to the single vector equation for the electric vector field $\vec{E}(\vec{r},t)$

$$\vec{E}_{tt} - c^2[\Delta_r \vec{E} - \vec{\nabla}_r(\vec{\nabla}_r \cdot \vec{E})] = -\frac{1}{\epsilon_0}\vec{P}_{tt}. \tag{3}$$

Here we assume that the medium is homogeneous but not isotropic, and that only its linear response, namely $\chi_{jn}^{(1)}$, is frequency dependent; moreover losses are assumed to be negligibly small. Thus the dielectric polarization field components P_j are related to the electric field by the standard formula (summation over repeated indexes is understood)

$$P_j(\vec{r},t) = \epsilon_0 \int_{-\infty}^{t} dt_1 \chi_{jn}^{(1)}(t-t_1) E_n(\vec{r},t_1) + \epsilon_0 \chi_{jnm}^{(2)} E_n(\vec{r},t) E_m(\vec{r},t) \quad . \tag{4}$$

The way to proceed further is via the widely used multiscale (or slowly varying amplitude approximation) method (see for instance (Degasperis, 2009) and references quoted there). The starting point is the following approximate expression of the solution (here *c. c.* means complex conjugate)

$$\begin{aligned} E_j(\vec{r},t) &= \eta[A^{(1)}(\vec{\xi},\tau)B_j^{(1)} e^{i(\vec{k}_1\cdot\vec{r}-\omega_1 t)} + A^{(2)}(\vec{\xi},\tau)B_j^{(2)} e^{i(\vec{k}_2\cdot\vec{r}-\omega_2 t)} \\ &+ A^{(3)}(\vec{\xi},\tau)B_j^{(3)} e^{i(\vec{k}_3\cdot\vec{r}-\omega_3 t)}] + c.c. + O(\eta^2) \ , \end{aligned} \tag{5}$$

where η is a small parameter which enters also in the scaled spatial co-ordinates $\vec{\xi} = \eta\vec{r}$ and in the slow time variable $\tau = \eta t$. This expression shows that the electric field is the superposition of three quasi–monochromatic waves, namely of three carrier waves which are modulated by the slowly varying amplitudes $A^{(\alpha)}$, α =1, 2, 3. Moreover, we have additionally assumed that only the wave amplitudes are affected by the nonlinear dynamics but not their state of polarization, so that the three vectors $\vec{B}^{(\alpha)}$, α = 1, 2, 3 are taken co-ordinate and time independent while the three dynamical variables $A^{(\alpha)}(\vec{\xi},\tau)$, α = 1, 2, 3 are just scalars. The wave–number vectors k_{1j}, k_{2j}, k_{3j}, their corresponding frequencies ω_1, ω_2, ω_3, together with the polarization state vectors $B_j^{(1)}, B_j^{(2)}, B_j^{(3)}$ satisfy the dispersion relation

$$(\omega^2 - c^2\vec{k}\cdot\vec{k})B_j + c^2\vec{k}\cdot\vec{B}k_j + \omega^2\hat{\chi}_{jn}^{(1)}(\omega)B_n = 0 \, , \tag{6}$$

where the function $\hat{\chi}_{jn}^{(1)}(\omega)$ is the Fourier transform

$$\hat{\chi}_{jn}^{(1)}(\omega) = \int_0^{+\infty} dt e^{i\omega t} \chi_{jn}^{(1)}(t) \quad . \tag{7}$$

It now remains to insert the expression (5) into the Maxwell's equation (3) and to expand the resulting formula in powers of the small perturbative parameter η. We omit detailing this computation and we limit ourselves to the following remarks. At first order, $O(\eta)$, one merely finds that wave numbers, frequencies and polarization state vectors of the three fundamental harmonics (see Eq. (5)) satisfy the dispersion relation (6). The resonance conditions (1) play a crucial role at the next order, $O(\eta^2)$, as they imply the coupling between the three wave amplitudes. Moreover, since the quadratic nonlinearity implies that all harmonics of the form $\exp\{i[\alpha_1(\vec{k}_1\cdot\vec{r}-\omega_1 t)+\alpha_2(\vec{k}_2\cdot\vec{r}-\omega_2 t)\}$ come into play, with any integer α_1 and α_2, one has to assume also that the dispersion relations of the medium are satisfied only for the three cases (α_1 = ±1, α_2 = 0), (α_1 = 0, α_2 = ±1) and (α_1 = α_2 = ±1). This condition guarantees that all higher harmonics are in the $O(\eta^2)$ term in the expression (5) and can therefore be omitted. The resulting $O(\eta^2)$ equations which are derived this way are then

$$\frac{\partial A_1}{\partial \tau} + \vec{v}_1 \cdot \vec{\nabla}_\xi A_1 = i\gamma_1 A_2^* A_3$$

$$\frac{\partial A_2}{\partial \tau} + \vec{v}_2 \cdot \vec{\nabla}_\xi A_2 = i\gamma_2 A_1^* A_3 \tag{8}$$

$$\frac{\partial A_3}{\partial \tau} + \vec{v}_3 \cdot \vec{\nabla}_\xi A_3 = i\gamma_3 A_1 A_2 .$$

Here the vectors $\vec{v}_1, \vec{v}_2, \vec{v}_3$ are the group velocities corresponding to the three carrier waves while the coefficients γ_1 , γ_2 , γ_3 are expressions in terms of the three fundamental harmonics wave numbers and polarization state vectors, and, of course, also of the linear and quadratic susceptibility coefficients $\chi_{jn}^{(1)}$ and $\chi_{jnm}^{(2)}$. This fully tridimensional three wave resonant interaction model has been investigated by Kaup (Kaup, 1981). Here we consider the reduced case in which the three amplitudes A_1 , A_2 , A_3 depend upon only two independent variables. Since the partial differential equations of the system (8) are of the first order, the four variables ξ_1 , ξ_2 , ξ_3 , τ play a similar role. Hence the choice of two independent variables out of the four may be dictated by the specific physical context under consideration. Thus one may describe temporal dynamics by choosing for instance the space and time coordinates $\xi_1 = \xi$ and τ, or spatial dynamics by choosing instead the variables ξ_1 and ξ_2. In this section we adopt the first notation by giving the variable τ the meaning of time. Finally, we prefer to transform amplitudes and co-ordinates so as to display the characteristic coefficients δ_1 , δ_2 , δ_3 which are proportional to the inverse of the group velocities, and to set the coupling constants equal to unit, $\gamma_\alpha = 1$, in (8) so as to write the TWI model equations in the dimensionless form

$$\frac{\partial A_1}{\partial \xi} + \delta_1 \frac{\partial A_1}{\partial \tau} = iA_2^* A_3$$

$$\frac{\partial A_2}{\partial \xi} + \delta_2 \frac{\partial A_2}{\partial \tau} = iA_1^* A_3 \tag{9}$$

$$\frac{\partial A_3}{\partial \xi} + \delta_3 \frac{\partial A_3}{\partial \tau} = iA_1 A_2 .$$

With no loss of generality, we shall write Eqs. (9) in a coordinate system such that $\delta_1 = 0$. Moreover, we consider the case $0 < \delta_3 < \delta_2$. This system of equations is not only of great interest because of its broad applicability, but it exhibits quite special mathematical properties. In fact it has been discovered (Zakharov & Manakov, 1973) that it is an *integrable* Hamiltonian system with the implication that it can be investigated by the spectral methods of soliton theory both in the class of solutions which are well localised (as for bright solitons) and in the class of solutions with nonvanishing values at infinity (as for dark solitons). In particular, this model has explicitly known solutions and infinitely many conservation laws (after early studies (Armstrong et al., 1970; Bers, 1975), for a review paper see (Kaup, 1979) and, more recently (Calogero & Degasperis, 2004; Degasperis & Lombardo, 2006; 2009)). Conservation laws are related to symmetries, namely to transformations of the two independent variables ξ and τ, and the dependent variables A_1 , A_2 , A_3, which leave the TWI

equations (9) invariant. As these transformations depend upon one or more arbitrary parameters, one may insert additional parameters into the expression of an explicit solution by just transforming this solution. Because of this practical use of symmetries, we report here a few of them. Moreover, we also report below, for some of these symmetries, their associated conservation laws which are derived by standard technique from the Lagrangian density

$$\mathcal{L} = \frac{1}{4i}\sum_{j=1}^{3} A_j^*(A_{j\xi} + \delta_j A_{j\tau}) - \frac{1}{2}A_1 A_2 A_3^* + c.c.. \tag{10}$$

To each of these symmetries it corresponds the local conservation law

$$\rho_\tau + \beta_\xi = 0 \tag{11}$$

which implies that, if the evolution variable is τ, the integral

$$R = \int_{-\infty}^{+\infty} d\xi \rho(\xi, \tau) \tag{12}$$

is the conserved quantity since it is τ − independent. On the other hand, if instead the variable ξ is the evolution variable (as in the case this is the spatial transverse co-ordinate), then the integral

$$B = \int_{-\infty}^{+\infty} d\tau \beta(\xi, \tau) \tag{13}$$

is the conserved quantity since it is ξ − independent. The conserved quantity among R and B which should be used depends of course on the physical process under investigation. The simplest symmetries are:

1. translation of the variable ξ, $A_j(\xi,\tau) \rightarrow A_j'(\xi,\tau) = A_j(\xi + a,\tau)$ whose associated conserved quantity is

$$P = \frac{1}{4i}\int_{-\infty}^{\infty}\sum_{j=1}^{3}\delta_j A_j^* A_{j\xi} d\xi + c.c., \tag{14}$$

   if the evolution variable is τ, or, if the evolution variable is instead ξ, the appropriate conserved quantity is

$$J = \int_{-\infty}^{\infty}(\frac{1}{4i}\sum_{j=1}^{3}\delta_j A_j^* A_{j\tau} - \frac{1}{2}A_1 A_2 A_3^*) d\tau + c.c.. \tag{15}$$

2. translation of the variable τ, $A_j(\xi,\tau) \rightarrow A_j'(\xi,\tau) = A_j(\xi,\tau + b)$ whose associated conserved quantity is

$$E = \int_{-\infty}^{\infty}(\frac{1}{4i}\sum_{j=1}^{3}A_j^* A_{j\xi} - \frac{1}{2}A_1 A_2 A_3^*) d\xi + c.c. \ , \tag{16}$$

   if the evolution variable is τ, or, if the evolution variable is instead ξ, the appropriate conserved quantity is

$$H = \frac{1}{4i}\int_{-\infty}^{\infty}\sum_{j=1}^{3}\delta_j A_j^* A_{j\tau} d\tau + c.c. \ . \tag{17}$$

3. phase translations, $A_1(\xi,\tau) \rightarrow A_1'(\xi,\tau) = \exp(i\theta_1)A_1(\xi,\tau)$, $A_2(\xi,\tau) \rightarrow A_2'(\xi,\tau) = \exp(i\theta_2)A_2(\xi,\tau)$, $A_3(\xi,\tau) \rightarrow A_3'(\xi,\tau) = \exp(i\theta_1 + i\theta_2)A_3(\xi,\tau)$ whose two associated conserved quantities are the well known Manley-Rowe invariants

$$M_{13} = M_1 + M_3 = \frac{1}{2}\int_{-\infty}^{\infty}\left(\delta_1 |A_1|^2 + \delta_3 |A_3|^2\right)d\xi,$$

$$M_{23} = M_2 + M_3 = \frac{1}{2}\int_{-\infty}^{\infty}\left(\delta_2 |A_2|^2 + \delta_3 |A_3|^2\right)d\xi \quad , \tag{18}$$

if the evolution variable is τ, or, if the evolution variable is instead ξ, the appropriate Manley-Rowe invariants read

$$I_{13} = I_1 + I_3 = \frac{1}{2}\int_{-\infty}^{\infty}\left(|A_1|^2 + |A_3|^2\right)d\tau,$$

$$I_{23} = I_2 + I_3 = \frac{1}{2}\int_{-\infty}^{\infty}\left(|A_2|^2 + |A_3|^2\right)d\tau \quad . \tag{19}$$

Two more symmetries which may turn out to be useful are the scale transformation $A_j(\xi,\tau) \rightarrow A_j'(\xi,\tau) = pA_j(p\xi, p\tau)$, where p is a real arbitrary parameter, and the characteristic phase transformation $A_1(\xi,\tau) \rightarrow A_1'(\xi,\tau) = \exp[iq(\delta_2 - \delta_3)\xi_1]A_1(\xi,\tau)$, $A_2(\xi,\tau) \rightarrow A_2'(\xi,\tau) = \exp[iq(\delta_3 - \delta_1)\xi_2]A_2(\xi,\tau)$, $A_3(\xi,\tau) \rightarrow A_3'(\xi,\tau) = \exp[-iq(\delta_1 - \delta_2)\xi_3]A_3(\xi,\tau)$, where q is an arbitrary real parameter and $\xi_j = \tau - \delta_j\xi$ are the characteristic co-ordinates.

Several explicit soliton solutions, of both bright and dark type, of the TWI equations (9) have been computed by algebraic construction methods, see (Degasperis & Lombardo, 2009) and references quoted there, and some of them are detailed in the following sections with the purpose of displaying their relevance to special optical processes.

On the applicative side, the three-wave resonant interaction has been extensively studied in the context of nonlinear optics, since it applies to parametric amplification, second harmonic generation and frequency conversion, stimulated Raman and Brillouin scattering and light speed control (Taranenko & Kazovsky, 1992; Ibragimov & Struthers, 1996; Ibragimov et al., 1998; Picozzi & Haelterman, 1998).

3. Frequency conversion

Optical parametric amplification in quadratic nonlinear crystals has been studied since the invention of the laser, as it provides a versatile means of achieving widely tunable frequency conversion (Cerullo & De Silvestri, 2003). In parametric processes, the effective interaction length of short optical pulses is limited by temporal walk-off owing to chromatic dispersion, or group velocity mismatch (GVM) (Armstrong et al., 1970; Akhmanov et al., 1992).

Compression and amplification of ultra-short laser pulses in second harmonic and sum-frequency (SF) generation in the presence of GVM was theoretically predicted (Wang & Dragila, 1990; Stabinis et al., 1991) and observed in several experiments (Wang & Luther-Davies, 1992; Chien et al., 1995). The conversion efficiency of generated SF pulses may be optimised (Ibragimov & Struthers, 1996; 1997; Ibragimov et al., 1998; 1999; Fournier et al., 1998) by operating in the soliton regime (Zakharov & Manakov, 1973; Kaup, 1976). In fact,

the temporal collision of two short soliton pulses in a quadratic nonlinear crystal may efficiently generate a short, time-compressed SF pulse (Ibragimov & Struthers, 1996). However this SF pulse is unstable: its energy decays back into the two incident pulses after a relatively short distance.

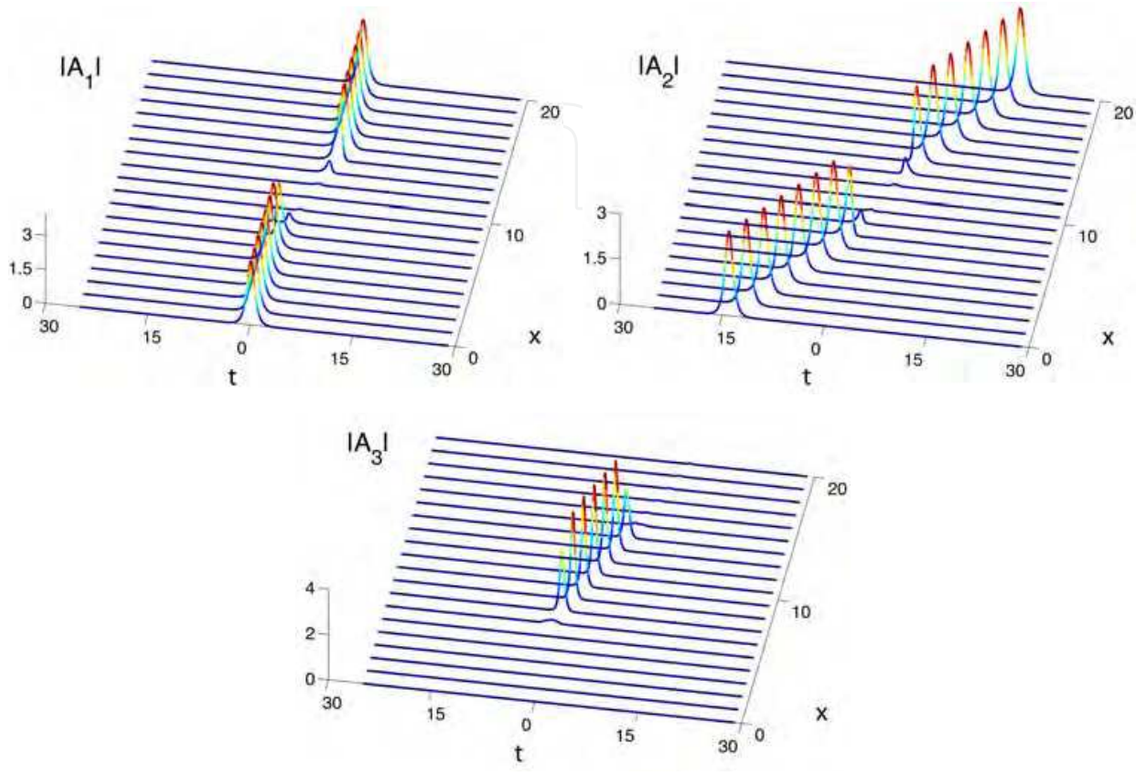

Fig. 1. Sum-frequency generation at ω_3 from the parametric interaction of two short optical signals at ω_1 and ω_2. The characteristic delays are $\delta_1 = 0$, $\delta_2 = 2$, $\delta_3 = 1$.

Figure 1 illustrates a typical example of the efficient SF parametric interaction of two short optical pulses in the soliton regime (Ibragimov & Struthers, 1996). At the crystal input, two isolated soliton pulses A_1 and A_2 with frequencies ω_1 and ω_2 propagate with speeds v_1 and v_2. Whenever the faster pulse overtakes the slower one, an idler pulse A_3 at the SF $\omega_1 + \omega_2$ is generated and propagates with the linear speed v_3. Depending on the time widths and intensities of the input pulses, the temporal duration of the SF pulse is reduced with respect to the input pulse widths. Correspondingly, the SF pulse peak intensity grows larger than the input pulse intensities. Figure 1 shows that, eventually, the SF idler pulse decays back into the two original isolated pulses at frequencies ω_1 and ω_2. Note that the shapes, intensities and widths of the input pulses are left unchanged in spite of their interaction. As shown in Ref. (Ibragimov & Struthers, 1996), the above discussed SF pulse generation process may be analytically described in terms of soliton solutions of Eqs. (9) (Zakharov & Manakov, 1973; Kaup, 1976). In the notation of Eqs. (9), the complete three–wave dynamics reads as:

$$A_1 = -i\frac{\Delta}{4p}\frac{\delta_2 - \delta_3}{\delta_2\delta_3}A_2^* A_3,$$

$$A_2 = i\frac{4p\delta_3}{\Delta}\sqrt{\frac{\delta_2}{\delta_2-\delta_3}}e^{iq_2\tau_2}exp[-2i\frac{\delta_3}{\delta_2-\delta_3}(k-ip)\tau_2],$$

$$A_3^* = i\frac{4p\delta_2}{\Delta}\sqrt{\frac{\delta_3}{\delta_2-\delta_3}}e^{iq_3\tau_3}exp[2i\frac{\delta_2}{\delta_2-\delta_3}(k+ip)\tau_3], \tag{20}$$

where

$$\Delta = 1+exp(-\frac{4p\delta_3}{\delta_2-\delta_3}\tau_2)+exp(-\frac{4p\delta_2}{\delta_2-\delta_3}\tau_3) \tag{21}$$

$$q_n = q(\delta_{n+1}-\delta_{n+2}), n = 1,2,3 mod(3),$$

$$\tau_n = -\tau+\delta_n\xi. \tag{22}$$

For a given choice of the characteristic linear group velocities, we are left with the three parameters p, k, q. The parameter p is associated with the re-scaling of the wave amplitudes, and of the coordinates τ and ξ. Here the value of k and q adds a phase shift which is linear in both τ and ξ.

The decay of the SF pulse which is shown in Fig. 1 may be a significant drawback in practical applications, since it implies that a given nonlinear crystal length yields efficient conversion for a limited range of input pulse intensities and time widths only. The parametric sum frequency conversion of an ultra-short signal and a quasi-CW background pump-control may be exploited as a means to reduce or even eliminate the decay of the generated idler wave (Conforti et al., 2007). In the presence of GVM, the parametric SF conversion of an ultra-short optical signal and a quasi-CW pump generally leads to the generation of a low-intensity and relatively long idler pulse, whose duration is associated with the interaction distance in the crystal.

This scenario changes dramatically in the soliton regime. Figure 2 illustrates the efficient generation of a stable, ultra-short SF idler pulse from the parametric SF conversion of a properly prepared ultra-short signal and a CW background control with an arbitrary intensity level. In Fig. 2 we injected in the quadratic nonlinear crystal the short signal at frequency ω_2, along with a delayed and relatively long pump-control pulse at frequency ω_1. Initially, the two pulses propagate uncoupled; as soon as the faster pulse starts to overlap in time with the slower quasi-CW control, their nonlinear mixing generates a short SF idler pulse. The sum frequency process displayed in Fig. 2 can be analytically explained and explored in terms of stable TWIS (Three Wave Interaction Soliton) solutions (Degasperis et al., 2006).

In the notation of Eqs. (9), the properly prepared ultra–short pulse is a ZM single–wave soliton pulse (Zakharov & Manakov, 1973) at frequency ω_2; it reads as

$$A_1 = 0, \quad A_2 = 2P\sqrt{\rho\delta_2\delta_3}\,\frac{e^{i\rho\phi\tau_2}}{\cosh(2P\rho\tau_2)}, \quad A_3 = 0, \tag{23}$$

where

$$\rho = \delta_3/(\delta_2-\delta_3), \ \tau_2 = -\tau+\delta_2\xi. \tag{24}$$

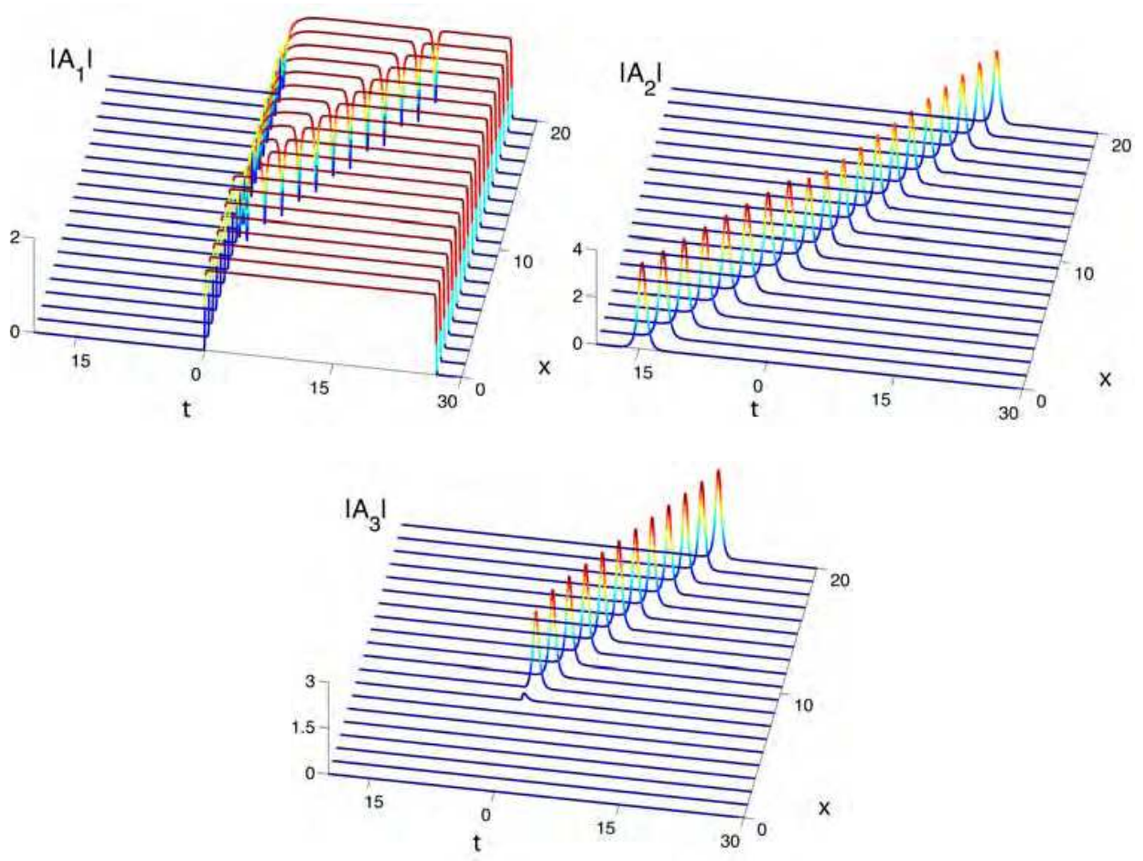

Fig. 2. Sum-frequency generation at ω_3 from the parametric interaction of a short pulse at ω_2 and a quasi-CW control at ω_1. The characteristic delays are $\delta_1 = 0$, $\delta_2 = 2$, $\delta_3 = 1$.

For a given choice of the three linear group velocities, or characteristic delays δ_j, the above ZM soliton is determined in terms of the two real parameters $P > 0$, ϕ. The parameter P fixes both the soliton peak amplitude and its temporal width. Whereas the parameter ϕ corresponds to a phase shift which is linear in both τ and ξ. On the other hand, the generic input quasi CW signal at frequency ω_1 may be described as

$$A_1 = \frac{Ce^{-i\gamma\tau}}{2}[\tanh(\frac{\tau-\tau_i}{\tau_r}) - \tanh(\frac{\tau-\tau_f}{\tau_r})], \quad A_2 = 0, \quad A_3 = 0, \tag{25}$$

where C is the complex amplitude and γ is the frequency shift with respect to ω_1 of the quasi-CW signal; τ_i (τ_f) and τ_r are the switch–on (switch–off) time and the rise/fall time of the quasi–CW signal, respectively. We consider the case in which $|C|^2 < P^2\delta_2\delta_3$.

When the faster short pulse, pre-delayed with respect to the slower quasi-CW pump at frequency ω_1, overtakes the background (at $\tau = 0$, in Fig. 2), their collision leads to the generation of a short idler pulse at the SF ω_3. Additionally, a dip appears in the quasi CW control; whereas the intensity, duration and propagation speed of the input wave at frequency ω_2 are modified. Indeed, the signal-pump interaction generates a stable TWIS simulton (Degasperis et al., 2006). In the notation of Eqs. (9), the TWIS simulton solution reads as

$$A_1 = \{1 + \frac{2pb^*}{|b|^2 + a^2}[1 - \tanh[B(-\tau + \delta\xi)]]\}\frac{ia\,g_1 \exp(iq_1\tau_1)}{g(\delta_2 - \delta_3)}$$

$$A_2 = \frac{2pa}{\sqrt{|b|^2 + a^2}}\frac{g_2}{g(\delta_2 - \delta_3)}\frac{\exp[i(q_2\tau_2 + \chi\tau + \omega\xi)]}{\cosh[B(-\tau + \delta\xi)]},$$

$$A_3 = \frac{-2pb^*}{\sqrt{|b|^2 + a^2}}\frac{g_3}{g(\delta_2 - \delta_3)}\frac{\exp[-i(q_3\tau_3 - \chi\tau - \omega\xi)]}{\cosh[B(-\tau + \delta\xi)]}, \tag{26}$$

where

$$b = (Q-1)(p + ik/Q), \quad r = p^2 - k^2 - |a|^2,$$

$$Q = \frac{1}{p}\sqrt{\frac{1}{2}[r + \sqrt{r^2 + 4k^2p^2}\,]},$$

$$B = p[\delta_2 + \delta_3 - Q(\delta_2 - \delta_3)]/(\delta_2 - \delta_3),$$

$$\delta = 2\delta_2\delta_3/[\delta_2 + \delta_3 - Q(\delta_2 - \delta_3)],$$

$$\chi = k[\delta_2 + \delta_3 - (\delta_2 - \delta_3)/Q]/(\delta_2 - \delta_3),$$

$$\omega = -2k\delta_2\delta_3/(\delta_2 - \delta_3)\ ,\ \tau_n = -\tau + \delta_n\xi$$

$$q_n = q(\delta_{n+1} - \delta_{n+2}),\ ,\ g_n = |(\delta_n - \delta_{n+1})(\delta_n - \delta_{n+2})|^{-1/2}$$

$$g = g_1 g_2 g_3\ , n = 1,2,3\ mod(3). \tag{27}$$

For a given choice of the characteristic linear group velocities, we are left with the four parameters p, a, k, q. The parameter p is associated with the re-scaling of the wave amplitudes, and of the coordinates τ and ξ. Whereas a measures the amplitude of the CW background in wave A_1 (namely $a\sqrt{\delta_2\delta_3}$). The value of k is related to the soliton wavenumber. The parameter q simply adds a phase shift which is linear in both τ and ξ (see (Degasperis et al., 2006) for parameter details).

It is remarkable that we may analytically predict the parameters p, k, q, a of the generated TWIS from the corresponding parameters of the input single wave TWIS and the complex amplitude of the pump control. This can be achieved by supposing that the input TWIS adiabatically (i.e., without emission of radiation) reshapes into a new TWI simulton after its collision with the quasi-CW pump at a given point in time (say, at $\tau = 0$). Under this basic hypothesis, the conservative nature of the three-wave interaction permits us to suppose that: i) the energy I_{23} (19) of the input TWI soliton is conserved in the generated TWI simulton; ii) the phase of the ω_2 frequency components of the input TWI soliton and of the generated TWI simulton is continuous across their time interface (i.e., at $\tau = 0$); iii) the amplitude and phase of the control pump C coincide with the corresponding values of the asymptotic plateau of the generated TWI simulton component at frequency ω_1. By imposing the above three conditions, after some straightforward calculations we obtain the following relations that relate the parameters of the incident and of the transmitted TWIS

$$p = P,\ a\sqrt{\delta_2\delta_3} = |C|,\ q(\delta_2 - \delta_3) = \gamma,\ q(\delta_2 - \delta_3) - 2k = \phi, \tag{28}$$

with the restriction $|C| < P\sqrt{\delta_2\delta_3}$.

As an example, in Fig. 2 the input TWI soliton at frequency ω_2 is described by Eqs. (23) with P = 1.3, ϕ = 0, and the background control amplitude is C = 1.7. After the collision with the CW background, the above equations predict that the generated TWIS is described by Eqs. (26), with p = 1.3, q = 0, k = 0, and a = 1.2. The accuracy of this prediction is well confirmed by its comparison with the numerical solutions of the TWI Eqs. (9). Indeed, Fig. 3 compares the numerical and the analytical evolutions (along the crystal length ξ) of the energy, the pulse duration and the velocity of the idler and signal pulses which correspond to the case shown in Fig. 2. We performed further extensive numerical simulations, which confirmed the general validity of the above described adiabatic transition model for TWIS generation upon collision with a CW background.

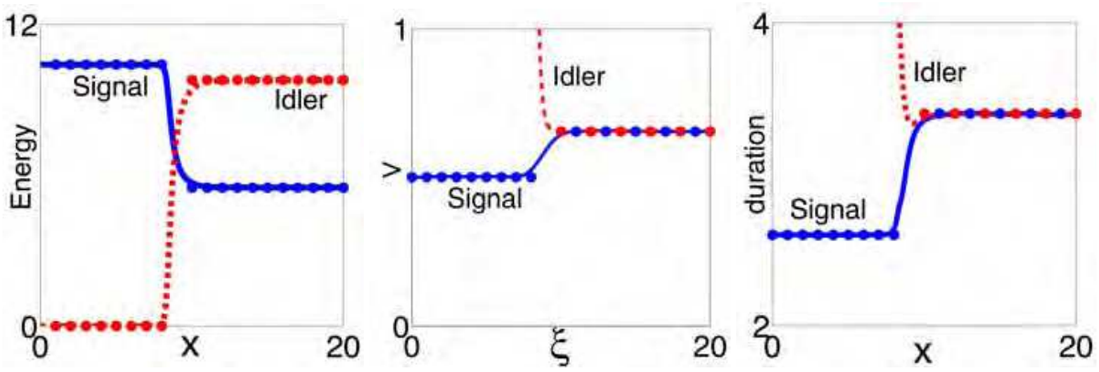

Fig. 3. Numerical evolution (lines) and theoretical predictions (circles) of energy, pulse duration and velocity of idler and signal waves reported in Fig.2.

Indeed, by increasing or decreasing the CW background amplitude $|C|$ in the range [0, $p\sqrt{\delta_2\delta_3}$], we observed that stable TWISs with different velocity, duration and energy distributions may be adiabatically shaped. The important consequence of this result is that, by means of Eqs. (26)–(28), we may analytically predict and control the characteristics of the generated idler pulse (namely, its velocity, time duration and energy) simply as a function of the intensity level of the CW pump. Moreover, we would like to emphasize that the stability of the whole SF idler conversion process is ensured by the underlying stability of the generated TWIS (Conforti et al., 2006).

4. Ultrafast pulse train generation

Efficient mechanisms for the generation of high–contrast, ultra–short pulse trains are of interest in a broad range of domains, such as time–resolved spectroscopy and microscopy, selective femtosecond chemistry, quantum coherent control in high–field physics, and optical communications. Relevant application examples include quantum–path control of high–harmonic generation (Zhang et al., 2007); multi–pulse excitation of atoms, molecules, and solids (Weiner et al., 1990); multiple–laser–pulse excitation of high–gradient plasma accelerators (Umstadter et al., 1994); high–fluence THz wave–train generation for radar, microwave (Liu et al., 1996) and optical communication systems. Several techniques for

generating trains of ultra–short pulses at repetition rates beyond those achievable by active laser mode locking or by means of electrically–controlled modulation have been explored in recent years. For example, linear pulse train generation techniques include the repetition–rate multiplication of a lower rate source by applying amplitude (Petropoulos et al., 2000; Yiannopoulos et al., 2003) or phase–spectral filtering (Longhi et al., 2000; Azana & Muriel, 2001; Caraquitena et al., 2007). Moreover, different all–optical techniques that may result in up to THz pulse train rates have also been proposed by using both quadratic and cubic nonlinear media. Consider for example induced modulation instability (Hasegawa, 1984; Coen & Haelterman, 2001), multiple four-wave-mixing (Pitois et al., 2002; Inoue et al., 2007), and backward quasi-phase-matched second harmonic generation (Conti et al., 1999; Conforti et al., 2005).

Here, we present a TWI nonlinear technique for the flexible generation of a train of ultra–short optical pulses with light-controlled time width, amplitude and repetition rate. This technique originates from the interaction of three waves at resonance (Baronio et al., 2008).

Let us first present numerical evidence of the train generation process. Figure 4 illustrates the possibility of obtaining an efficient modulation of the input CW signal into a train of ultra–short pulses, as a result of its parametric mixing with an ultra-short ZM soliton pulse at a different carrier wavelength. In particular, in Fig. 4 we numerically solved Eqs. (9), where the initial excitation conditions at $\xi = 0$ were provided by a quasi–CW signal at frequency ω_1 (a standing signal in a coordinate system where $\delta_1 = 0$) and a short ZM soliton pulse at frequency ω_2 (with delay parameter $\delta_2 > 0$). The two input pulses were pre-delayed, so that they could collide at some distance inside the crystal. Figure 4 shows that, as soon as the faster ZM soliton pulse starts to overlap in time with the slower quasi–CW signal, their parametric mixing leads to the generation of an idler short pulse at frequency ω_3. Additionally, Fig. 4 also shows that the TWI leads to a periodic oscillation with distance ξ of the intensity of the two short pulses at carrier frequencies ω_2 and ω_3. As a result, it turns out that the centre of mass of these two pulses periodically oscillates in time around an average value, which grows larger with distance according to a common average group velocity; this velocity is clearly (see Fig. 4) different from the group velocity of the incoming short pulse. As for the incoming CW signal, Fig. 4 also shows that a train of short pulses is carved on the CW background at frequency ω_1. Finally, Fig. 4 also illustrates that at the end of the three–wave interaction process the quasi–CW background at ω_1 is modulated into a sequence of ultra–short pulses, the soliton pulse at ω_2 returns back to its original shape, and the generated sum-frequency pulse at ω_3 vanishes.

Quite remarkably, we shall demonstrate that the entire three–wave interaction process which is displayed in Fig. 4 may be analytically represented in terms of particular analytical TWI solutions. As in the previous section, in the notation of Eqs. (9), the arbitrary input quasi CW signal at frequency ω_1 is given by expression (25) and the input ZM single–wave soliton pulse at frequency ω_2 by expression (23). We consider the case in which $|C|^2 > P^2\delta_2\delta_3$ and $\gamma = \phi$.

After the collision of the ZM pulse with the CW background, we surmise that their parametric interaction generates a three-wave trapponic soliton, which consists of a group-velocity locked bright-bright-dark triplet. Similar triplet solutions have been already considered in nonlinear optics in the form of simultons (Degasperis et al., 2006; Conforti et al., 2007) or boomerons (Conforti et al., 2006). Trappon soliton solutions of the TWI Eqs. (9) may be found as discussed in the recent analysis of Ref. (Calogero & Degasperis, 2005;

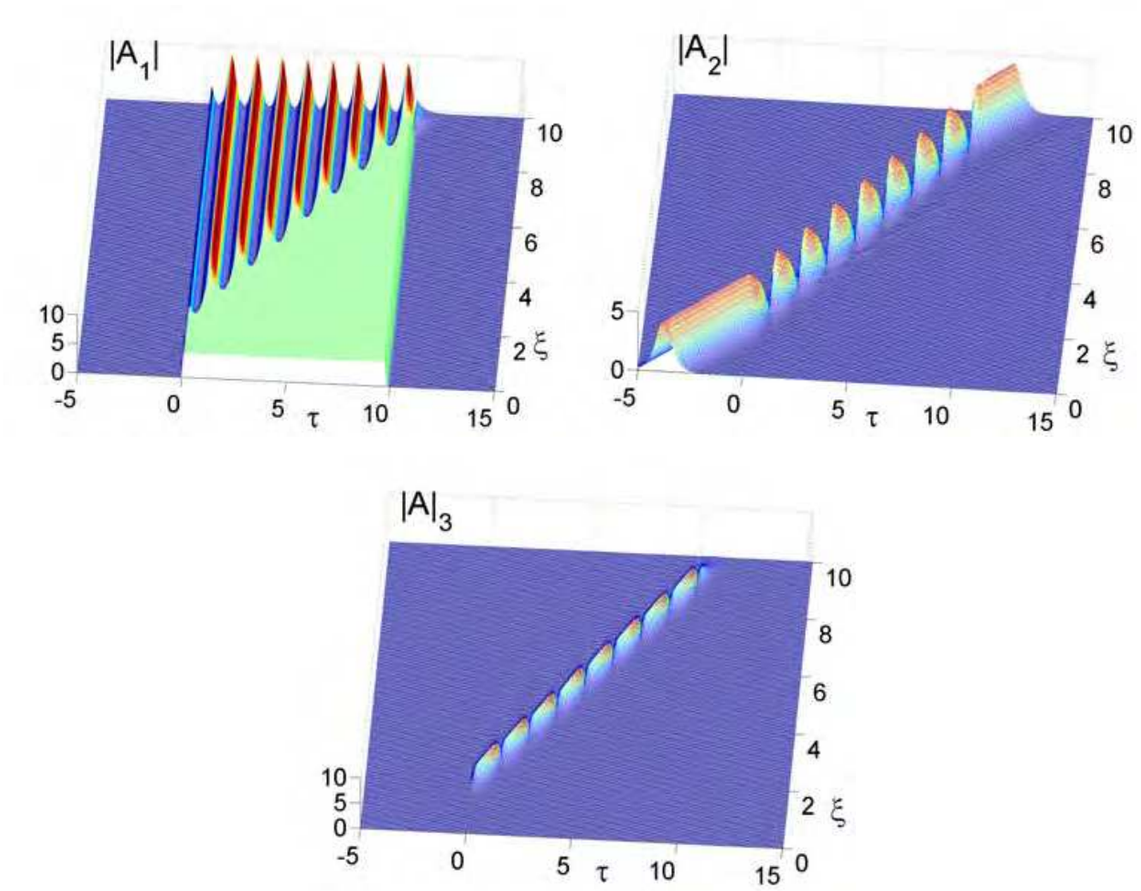

Fig. 4. Sum–frequency generation at ω_3 from the parametric interaction of a quasi–CW control at ω_1 and a short pulse at ω_2. The characteristic delays are $\delta_1 = 0$, $\delta_2 = 2$, $\delta_3 = 1$.

Degasperis et al., 2006). TWI trappons are characterized by a periodic (or trapped) spatio–temporal evolution of the energy distribution of the three waves, as well as of their locked propagation speed. As a result, the center of mass of a trappon also periodically oscillates within a limited time interval. As far as the potential applications are concerned, the most significant property of the trappon dynamics consists in the carving of a train of short pulses into the CW–background at frequency ω_1. Indeed the entire three–wave interaction dynamics after the collision of the short pulse with the CW background as shown by Fig. 4 may be analytically described in terms of the trappon solution

$$A_1 = ia\sqrt{\delta_2\delta_3}e^{iq_1\tau_1} - i\frac{\Delta}{4p}\left(\frac{\delta_2-\delta_3}{\delta_2\delta_3}\right)A_2^*A_3,$$

$$A_2 = -\frac{2p\delta_3}{\Delta}\sqrt{\frac{2\delta_2}{\delta_2-\delta_3}}e^{iq_2\tau_2}(H_+^* - H_-^*),$$

$$A_3^* = \frac{2p\delta_2}{\Delta}\sqrt{\frac{2\delta_3}{\delta_2-\delta_3}}e^{iq_3\tau_3}(H_+e^{i\beta} - H_-e^{-i\beta}), \tag{29}$$

where

$$\Delta = 1 + |H_+|^2 + |H_-|^2 - 2\cos(\beta)\mathcal{R}e(H_+ H_-^* e^{i\beta}),$$

$$H_\pm = e^{-(B\pm i\chi)\tau} e^{\frac{2\delta_2\delta_3}{\delta_2-\delta_3} p\xi},$$

$$\chi = \sqrt{a^2 - p^2},$$

$$B = p\left(\frac{\delta_2+\delta_3}{\delta_2-\delta_3}\right), \tan(\beta) = \sqrt{a^2 - p^2} / p,$$

$$\delta = \frac{2\delta_2\delta_3}{\delta_2+\delta_3},$$

$$q_n = q(\delta_{n+1} - \delta_{n+2}) \ , \ n = 1,2,3 mod(3),$$

$$\tau_n = -\tau + \delta_n \xi. \tag{30}$$

For a given choice of the characteristic linear velocities in Eqs. (9), the trappon solution of Eqs. (29) is completely determined by just three independent real parameters, namely p, q, a (with the restrictions that $p > 0$, $a > 0$ and $a^2 > p^2$). The parameter p is associated with the rescaling of the wave amplitudes, and of coordinates τ and ξ. Whereas a measures the amplitude of the CW background in wave A_1. The parameter q adds a phase shift which is linear in both τ and ξ.

The trappon solution (29) extends in time from $\tau = -\infty$ to $\tau = +\infty$ and at large distances (i.e., for $\xi \to +\infty$) it exhibits a time–periodic behavior. Nevertheless, as we shall see, Eqs. (29) exactly describe the mixing of the ZM soliton (23) with the quasi–CW (25) background signal over the finite interval $[\tau_i,\tau_f]$ (which correspond to the times of turning on and off the CW wave at frequency ω_1, respectively).

Indeed, one may analytically predict the characteristic parameters p, q, a of the generated TWI trappon from the corresponding P, ϕ parameters of the isolated input ZM soliton, and the complex amplitude C and the frequency shift γ of the CW signal. As we discussed in the previous section, it is sufficient to suppose that the input ZM soliton adiabatically (i.e., without emission of radiation) reshapes into a trappon soliton after its collision with the quasi–CW background at a given point in time (say, at $\tau = \tau_i$). In the spectral domain (Zakharov & Manakov, 1973) this hypothesis is equivalent to imposing that the input ZM soliton, after the collision with the CW background, transfers its discrete eigenvalue to the trappon soliton. In the frame of this basic hypothesis, the conservative nature of the three–wave interaction permits us to suppose that: i) the energy I_{23} (19) of the input TWI soliton is conserved in the generated trappon soliton; ii) the phase of the ω_2 frequency components of the input TWI soliton and of the generated TWI soliton varies in a continuous manner across their time interface (i.e., at $\tau = \tau_i$); iii) the amplitude and the phase of the CW background coincide with the corresponding values of the asymptotic plateau of the component at frequency ω_1 of the generated TWI trappon. The above three conditions, after some straightforward calculations, permit us to obtain the following equations that relate the parameters of the incident and the transmitted solitons (i.e., before and after the collision, respectively)

$$p = P,\ a\sqrt{\delta_2\delta_3} = |C|,\ q(\delta_2 - \delta_3) = \phi, \tag{31}$$

with the restrictions that $|C|^2 > P^2\delta_2\delta_3$ and $\gamma = \phi$. The above conditions define the matching relations among the amplitudes and the phases of both the input ZM soliton and of the CW signal which should be satisfied in order to excite the trapponic soliton. As an example, consider the case of Fig. 4, where the CW background control is described by Eqs. (25) with $C = 3$, $\gamma = 1$, and the input ZM soliton is obtained from Eqs. (23) with $P = 1.5$, $\phi = 1$. After the collision with the CW background, Eqs. (31) predict that the generated trappon is obtained from Eqs. (29) with $p = 1.5$, $q = 1$, and $a = 3/\sqrt{2}$. We confirmed the accuracy of this prediction by means of extensive comparisons of the analytical expression (29) with numerical solutions of the TWI Eqs. (9). For example, Fig. 5 displays both numerically computed and analytical evolutions for the energy I_2 (along the crystal length ξ) and for the output transverse profile of wave A_1 (along τ) (these correspond to the same interaction process previously shown in Fig. 4).

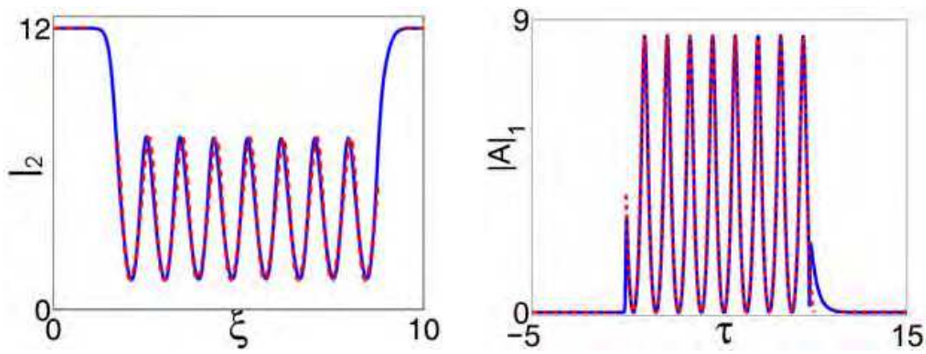

Fig. 5. Numerical evolution (continuous lines) and theoretical prediction from Eqs. (29) (dotted lines) of the energy at ω_2 and of the output pulse profile at ω_1 for the case of Fig. 4.

The amplitude profile of the generated train of ultra–short pulses at frequency ω_1 may be exactly described by performing the limit for $\xi \to +\infty$ of the first of Eqs. (29), which yields

$$|A_{1\infty}(\tau)| = |C|\,|1 - 4\cos(\beta)\frac{\sin(\pi\tau/T)\sin(\pi\tau/T - \beta)}{1 - \cos(\beta)\cos(2\pi\tau/T - \beta)}| \tag{32}$$

where $|C| = a\sqrt{\delta_2\delta_3}$ (see (28)), $\tan(\beta) = \sqrt{a^2 - p^2}/p$ (see (30)) and period $T = \pi/\sqrt{a^2 - p^2}$. Two different examples of the generated pulse trains as described by Eqs. (32) are shown in Fig. 6 a)–b).

Equation (32) provides relatively simple expressions that relate the parameters of the injected soliton pulse and CW background to the main features of the generated output pulse train. Indeed, $|A_{1\infty}|$ is a time periodic signal (with period T) with average value approximatively equal to $|C|$. Moreover, from Eqs. (32) one obtains that the peak amplitude of the generated pulses is $M = |C| + 2\sqrt{\delta_2\delta_3}\,P$; whereas the minimum amplitude is $m = |C| - 2\sqrt{\delta_2\delta_3}\,P$. Hence the maximum intensity contrast for the generated train is obtained for $|C| = 2P\sqrt{\delta_2\delta_3}$: in this case, the field amplitude at the minima vanishes and the peak amplitude reads as $M = 4\sqrt{\delta_2\delta_3}\,P$.

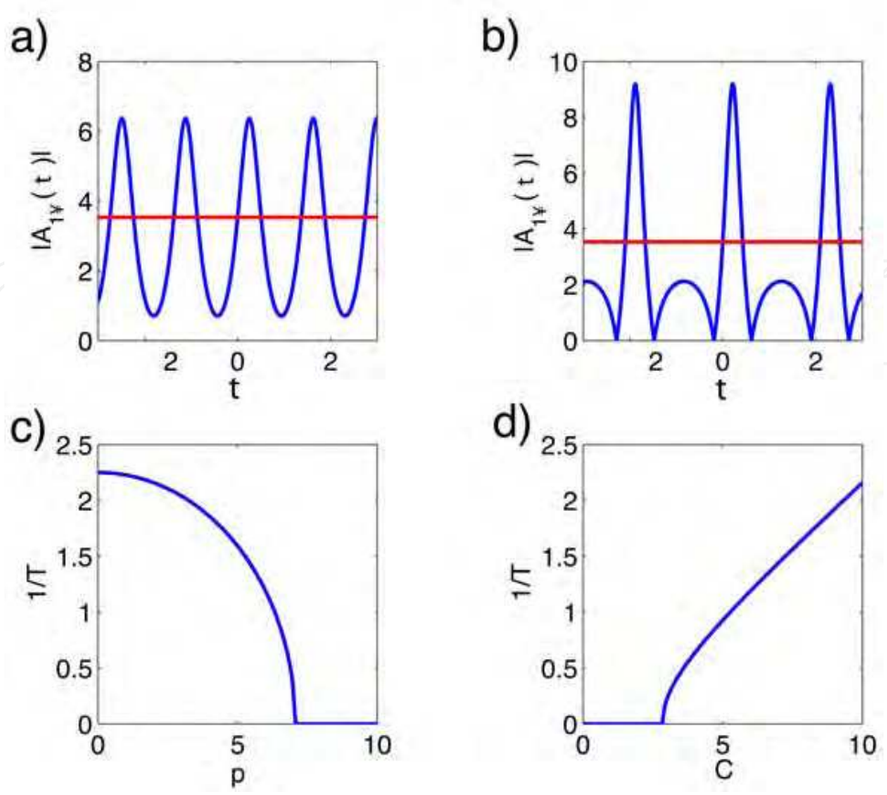

Fig. 6. Output pulse train (32) amplitude (blue line) and its time–average value (red line) for: a) $C = 2.5\sqrt{2}$,$P = 1$ and b) $C = 2.5\sqrt{2}$,$P = 2$; Pulse train frequency $f = 1/T$ c) vs. P ($C = 10$); and d) vs. C ($p = 2$).

In Figure 6 c)–d) we illustrate the analytically predicted dependence of the repetition rate of the ultra–short pulse train $R = 1/T = \sqrt{|C|^2/(\delta_2\delta_3) - p^2}\,/\,\pi$, as a function of the amplitudes of the input short pulse and of the CW signal, respectively. As it can be seen in Fig. 6 c), the repetition rate is the largest whenever the amplitude of the input soliton vanishes. Whereas there is a critical input soliton amplitude, above which the period of the generated pulse train diverges to infinity. On the other hand, Fig. 6 d) shows that when varying the CW background amplitude, a finite repetition rate is only obtained for amplitudes $|C|$ above a certain threshold level, and this rate grows larger with $|C|$ in a linear fashion. In fact, these thresholds define the borderlines of existence of TWI simulton triplets or TWI trappons excitations.

The above results show that the peak amplitude, the time width and the repetition rate of the pulse train which is generated at ω_1 may be controlled in a stable manner by simply adjusting the intensity level of the input CW signal $|C|$ and/or the amplitude level (hence the time width) P of the input short soliton pulse.

It is worth noting that the proposed method for generating pulse trains has a very high efficiency: in principle, the entire energy of the pump pulse A_1 may be converted into the pulse train. Indeed from (i) the energy conservation relation (19) and (ii) the fact that at the end of interaction $A_3 = 0$, it follows that the energy of the quasi-CW pulse is conserved before and after the collision with the control pulse A_2.

It should be pointed out that the generation process that we have described so far may be thought of as a way of "writing" a pulse train on a quasi CW signal. The opposite process of "erasing" such wave train to go back to a flat, quasi CW, signal is also possible. Indeed, it is easy to realize that this reverse process is well described in a similar way by the formation of the trappon soliton solution of the TWI Eqs. (9) which is obtained from the expression (29) via the invariance transformation $\xi \to -\xi$, $\tau \to -\tau$, $A_1 \to A_1$, $A_2 \to A_2$, $A_3 \to -A_3$.

5. Experimental observability

In this section, we discuss the experimental conditions for the practical observation of three wave solitons, with particular reference to their applications to frequency conversion and pulse train generation as discussed in the previous sections. It is interesting to notice that the three-wave soliton concept may be applied to describe the interaction between either three optical pulses in the time domain, or three beams in the spatial domain.

5.1 Temporal solitons

To be specific, let us consider the nonlinear *eee* interaction of two pulses, at $\lambda_1 = 1550$ nm and at $\lambda_2 = 3400$ nm, which mix in a 2 *cm* long periodically poled bulk Lithium Niobate crystal with about $28\mu m$ periodicity, to generate the sum-frequency pulse at $\lambda_3 = 1064$ nm. For perfect phase-matching with collinear geometry, one obtains the refraction indexes: $n_1 = 2.117$, $n_2 = 2.05$ and $n_3 = 2.134$, respectively. The corresponding group velocities satisfy the inequality $v_1 > v_3 > v_2$, namely $v_1 = 1.386 \times 10^8$ m/s, $v_3 = 1.374 \times 10^8$ m/s and $v_2 = 1.3615 \times 10^8$ m/s. In other words, the sum–frequency pulse group velocity is intermediate between the group velocities of the two input signals. This condition is crucial for the existence and stability of TWI soliton, simulton and trapponinc solutions. The effective nonlinear coefficient is $d_{33} = 25$ pm/V.

Whenever the input pulses are ZM single wave solitons, for instance pulses of about 200 *fs* temporal duration with peak intensity of a few hundreds of MW/cm^2, 100% energy conversion into a time compressed sum-frequency pulse is achievable at a certain point of the nonlinear crystal, for a proper ratio among the intensities of the two input fundamental pulses (Ibragimov & Struthers, 1996; 1997). The drawback is that, after a relatively short propagation distance, the generated pulse decays again in the two original fundamental solitons.

Whenever an input pulse is a ZM single wave soliton, i.e. a pulse of about 200 *fs* temporal duration with peak intensity of a few hundreds of MW/cm^2, and the other input signal is a quasi–continuous wave (say, with a $3ps$ time duration), their interaction leads to the generation of an ultra–short stable sum–frequency pulse of approximately the same time width (200 *fs*) of the incident short pulse. It is particularly significant that the peak intensity (and the group velocity) of the generated pulse may continuously evolve upon propagation through the crystal, from zero to a few hundreds of MW/cm^2 (v from v_3 to v_2), simply by varying the intensity of the quasi-CW background (Conforti et al., 2007). Such unique feature may enable to achieve the stable frequency conversion of short signal optical pulses, as well as the continuous control of the frequency conversion efficiency by adjusting the input intensity of the quasi-CW background pump wave.

In addition, the control of the CW pump power level also permits the highly efficient generation of a sum-frequency converted train of idler pulses which represent a time-

periodic copy of the input short signal pulse (Baronio et al., 2008). Whenever the peak intensity of the quasi–CW signal is higher than the peak intensity of the short ZM soliton pulse, the parametric mixing leads to the generation of a train of 250 *fs* pulses with a repetition rate of about 2*THz* and peak power levels of the order of a few hundreds of MW/cm^2. Again the peak amplitude, the time width and the repetition rate of the pulse train which is generated may be controlled in a stable manner by simply adjusting the intensity level of the input qusi-CW signal.
In practical terms, the upper limit to the frequency conversion and train generation processes offered by the present technique will be set by the limit of validity of Eqs. (9), which hold true in all three–wave physical systems whenever the presence of group velocity dispersion within each wave can be neglected.

5.2 Spatial solitons

As discussed in section 2, one could write the same TWI model Eqs. (9) where the independent coordinates are, instead of $\xi_1 = \xi$ and τ, the two spatial variables ξ_1 and ξ_2. In order to clearly distinguish this situation, involving the interaction between three spatial beams, from the previous cases involving short temporal pulses, and to maintain the same notation used in (Baronio et al., 2009), we name the longitudinal spatial coordinate $\xi_1 = z$ and the transverse spatial coordinate $\xi_2 = x$. Moreover, we also set in this case $A_{1,2,3} = \phi_{1,2,3}$. Note that the spatial beams under consideration are supposed to be wide enough so that diffraction (in analogy with group-velocity dispersion in the temporal case) may be neglected in the propagation of each individual beam, at least over their interaction distance. The interest in studying the spatial case is twofold: from one side it appears to be the simplest situation for providing experimental evidence of three wave soliton dynamics; from the practical viewpoint, spatial solitons in this framework might reveal interesting properties for beam shaping and switching.
Here we describe the set-up which led to the first experimental demonstration of laser beam reshaping by means of the three-wave ZM soliton effect in optics (Baronio et al., 2009).
To be precise, Fig. 7 illustrates the numerical optical scenario exploited to demonstrate the existence of ZM solitons. Here we show numerical simulations, with $\delta_1 = -\delta_2$ and $\delta_3 = 0$, illustrating the typical wave dynamics in the spatial $x - z$ plane in the presence of two electromagnetic beams ϕ_1 at λ_1, ϕ_2 at λ_2 and no beam ϕ_3 at λ_3 in $z = 0$ interacting in a quadratic nonlinear medium; that is, $\phi_1(x,0) \neq 0$, $\phi_2(x,0) \neq 0$, $\phi_3(x,0) = 0$.
Fig. 7.a shows the dynamics of the low–intensity linear regime: the beams at the two fundamental wavelengths λ_1 and λ_2 do not interact and propagate with their own characteristic directions associated with the respective spatial velocities v_1 and v_2.
Next, Fig. 7.b shows that, at intermediate input intensities, the beams at wavelengths λ_1 and λ_2 interact and generate a beam at λ_3. As the two fundamental waves overlap in space, the sum frequency wave ϕ_3 is generated. After the collision, the energy remaining in each input beam keeps propagating along the original direction corresponding to their linear wavevectors. Note that the collision between the input waves does not lead to any spatial shift in their propagation directions. In fact, in this situation it can be shown that no three-wave soliton is generated by the interaction process. According to the definition of a soliton as a discrete component of the spectrum that is obtained by means of the spectral transform

method (Zakharov et al., 1980; Zakharov, 1991), in Fig. 7.b the initial data $\phi_1(x, z = 0)$, $\phi_2(x, z = 0)$, $\phi_3(x, z = 0)$ is only composed of a continuum spectrum component (radiation) without any discrete spectrum component (solitons).

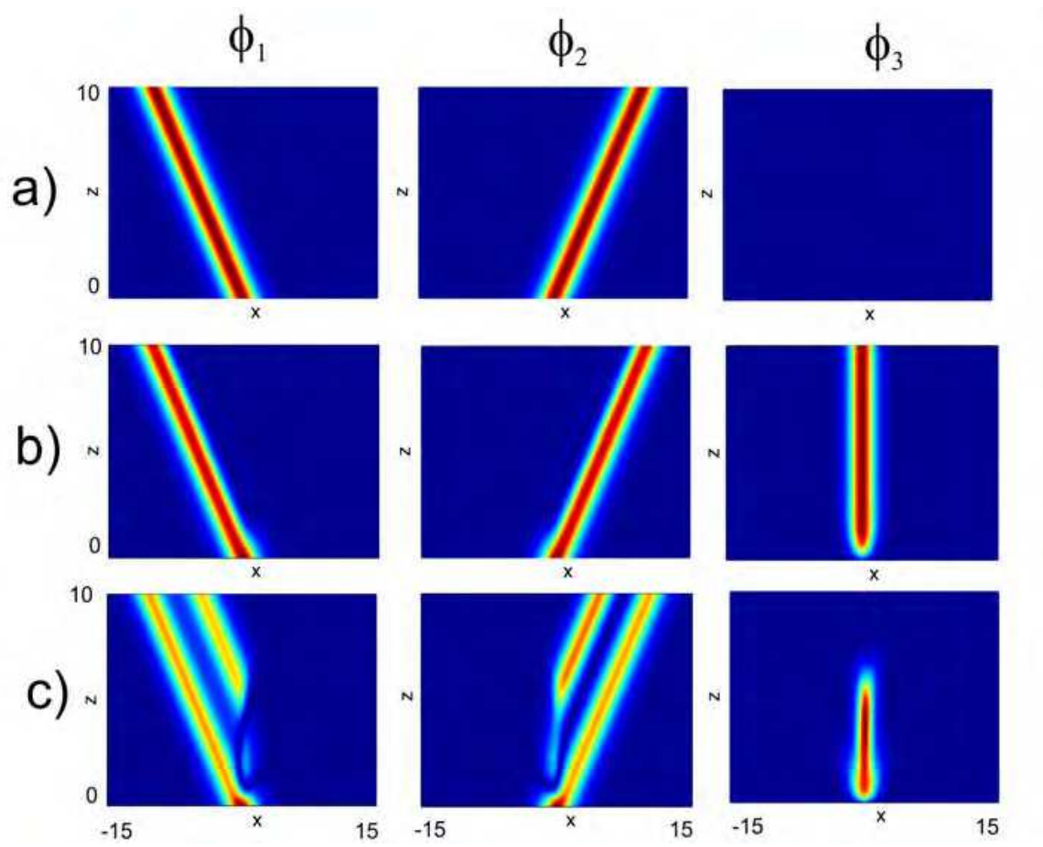

Fig. 7. Numerical $x - z$ TWI dynamics of waves at wavelengths λ_1 and λ_2 which mix to generate a field at the wavelength λ_3. (a) Linear, (b) frequency conversion, and (c) solitonic regime.

Finally, Fig. 7.c shows that, at relatively high input intensities, the interaction between the two input beams and the generated beam is qualitatively different from the previous cases. In fact, in this case the input fields contain a discrete soliton component along with a residual radiation spectrum. The solitonic behavior of the three wave interaction is not visible in the first part (i.e., the signal generation) of the interaction picture of Fig. 7.c, which is similar to what happens in Fig. 7.b: as in this case the residual input beams which keep propagating after generating the sum-frequency wave are composed by pure radiation. In fact, the presence of a soliton in the generated beam is revealed in its subsequent complete decay into the two waves, which is the spatial analog of the temporal soliton decay. From the point of view of the spectral transform of the optical field, we may say that in this case the initial data $\phi_1(x, z = 0)$, $\phi_2(x, z = 0)$, $\phi_3(x, z = 0)$ is composed of both a continuum spectrum component, or radiation, and a discrete spectrum component or soliton.

Another signature of the soliton presence in Fig. 7.c is the characteristic spatial shift that is observed between the two input soliton fundamental beams, and the output soliton fundamental beams that are generated from the decay of the soliton pump beam, with no change of the propagation direction before and after the three-wave interaction process. From another perspective, we may point out that if the generated beam was not a three-wave soliton, then its evolution could be predicted from a simple CW analysis. In this case one would not observe a sharp wave decay at a well-defined point along the crystal, but rather its continuous back-conversion into the two fundamental waves which would emerge from the process substantially wider with respect to the original input beams.
As a matter of fact, as in the case of temporal solitons, in the spatial case we may identify three separate interaction regimes. Namely, the linear, the frequency conversion, and the solitonic regime. In order to provide the experimental demonstration of the above discussed nonlinear dynamics, Ref. (Baronio et al., 2009) considered the optical spatial non–collinear scheme with type II second harmonic generation (SHG) in a birefringent KTP crystal. Two orthogonally polarized beams at frequency $\lambda_1 = \lambda_2 = \lambda = 1064$nm, E_λ^e and E_λ^o , were injected into the nonlinear birefringent medium to cross and overlap at the input face of the crystal. Each field was linearly polarized and aligned with a polarization eigenstate of the crystal. In the present scheme the two input waves required for the parametric processes to occur, and for the subsequent observation of solitonic decay, had tilted wave–fronts. In the overlapping area the harmonic $E_{\lambda/2}^e$ at $532nm$ was generated along a direction which maximized the conversion efficiency as it was fixed by the noncollinear phase–matching conditions. The sum–frequency harmonic propagation direction was found to be in between the directions of the two input waves. As the intensities of the input fields were varied in a suitable range ($1MW/cm^2 - 2.5GW/cm^2$), the TWI linear, frequency conversion, and solitonic regimes in the ordinary KTP plane were experimentally observed as reported in ref.(Baronio et al., 2009).

6. Conclusions

Introduced by a self-contained derivation in section 2 of the 1+1 dimensional equations ruling three-wave parametric interactions in dispersive and quadratic nonlinear optical crystals, in this chapter we presented an extensive review of their exact simulton solutions. Exploiting the properties of such solutions may have important practical applications to the parametric frequency conversion (e.g., sum and frequency difference generation) of short optical pulses. As discussed in section 3, a key property of simulton solutions consisting of two bright and one dark wave packet is that their common group velocity may be controlled in all-optical manner by adjusting the input energy distribution of its three wave components. We pointed out in section 3 that the simulton speed as well as the energy of its component waves may evolve in an adiabatic manner whenever one of their parameters (such as the input power of one of the waves) is varied at the crystal input. The above property permits to obtain a stable (i.e., independent of the precise crystal length or optical peak power) frequency conversion of relatively short isolated optical pulses when mixing them with quasi–CW pulses. In section 4, we have discussed how, by properly adjusting the power of the quasi–CW pulses, one may achieve a full modulation of this CW in a time-periodic replica of the input short pulse at a different frequency. We could provide simple

analytical expressions that permit to relate the time duration, the amplitude and the repetition rate of the generated pulse sequence with the input short pulse and CW. Finally, in section 5 we have outlined under which practical conditions it should be possible to achieve an experimental confirmation in commonly available quadratic nonlinear crystals of the theoretically predicted frequency conversion and pulse train generation effects. A first demonstration of nonlinear beam reshaping associated with three–wave interaction soliton properties was recently carried out in the spatial domain, and its peculiar properties have been discussed at the end of section 5.

7. References

Azana, J.; & Muriel, M. (2001) Temporal self-imaging effects: theory and application for multiplying pulse repetition rates, *IEEE J. Sel. Top. Quantum Electron.*, Vol. 7, pp. 728-744

Akjmanov, S.A.; Vysloukh, V.A.; & Chirkin, A.S. (1992) *Optics of Femtosecond Pulses* AIP, New York

Armstrong, J.A.; Jha, S.S.; & Shiren, N.S. (1970) Some effects of group-velocity dispersion on parametric interactions, *IEEE J. Quantum Electronics*, Vol. QE-6, pp. 123-129

Baronio, F.; Conforti, M.; Degasperis, A. & Wabnitz, S. (2008) Three-wave trapponic solitons for tunable high–repetition rate pulse train generation, *IEEE J. Quantum Electronics*, Vol. 44, pp. 542-546

Baronio, F.; Conforti, M.; Andreana, M; Couderc, V.; De Angelsi, C.; Wabnitz, S.; Barthelemy, A; & Degasperis, A. (2009) Frequency generation and solitonic decay in three-wave interactions, *Optics Express*, Vol. 17, pp 13889-13894

Bers, A. (1975) Linear waves and instabilities, *Plasma Physics-Les Houches 1972*. Edited by De Witt C. and Peyraud J., Gordon and Breach, New York, pp 113-215

Calogero, F. & Degasperis, A. (2004). New integrable equations of nonlinear Schrödinger type, *Studies Appl. Math.* Vol. 113, pp 91-137

Calogero, F. & Degasperis, A. (2005) Novel solution of the system describing the resonant interaction of three waves, *Physica D* , Vol. 200, pp. 242–256

Caraquitena, J.; Jiang, Z.; Leiard, D.E.; & Weiner, A.M. (1995). Tunable pulse repetition-rate multiplication using phase-only line-by-line pulse shaping, *Opt. Lett.*, Vol. 32, pp. 716-718

Cerullo, G. & De Silvestri, S. (2003) Ultrafast optical parametric amplifiers, *Rev. Sci. Instrum.*, Vol. 74, pp. 1–18

Chien, C.Y.; Korn, G.; Coe, J.S.; Mourou, G. & Craxton, R.S. (1995). Highly efficient secondharmonic generation of ultraintense Nd:glass laser pulses, *Phys. Rev. E*, Vol. 20, pp. 353-355

Coen, S. & Haelterman, M. (2001) Continuous-wave ultrahigh repetition rate pulse train generation through modulation instability in a passive fiber cavity, *Opt. Lett.*, Vol. 26, pp. 39–41

Conforti, M.; Locatelli, A.; De Angelis, C.; Parini, A.; & Trillo, S. (2005). Self-pulsing instabilities in backward parametric wave-mixing, *J. Opt. Soc. Am. B*, Vol. 22, pp. 2178-2184

Conforti, M.; Baronio, F.; Degasperis, A. & Wabnitz, S. (2006) Inelastic scattering and interactions of parametric three-Wave solitons, *Phys. Rev. E*, Vol. 74, pp. 0656021-4(R)

Conforti, M.; Baronio, F.; Degasperis, A. & Wabnitz, S. (2007). Parametric frequency conversion of short optical pulses controlled by a CW background, *Optics Express*, Vol. 15, Issue 19, pp. 12246-12251

Conti, C.; Assanto,G.; & Trillo, S. (1999). Cavityless oscillation through backward quasi-phasematched second-harmonic generation, *Opt. Lett.*, Vol. 24, pp. 1139-1141

Degasperis, A. & Lombardo, S. (2006). Exact solutions of the 3-wave resonant interaction equation, *Physica D*, Vol. 214, 157-168

Degasperis, A.; Conforti, M.; Baronio, F. &Wabnitz, S. (2006), Stable Control of Pulse Speed in Parametric Three-Wave Solitons, *Phys. Rev. Lett.* Vol. 97, No. 9, 093901-04

Degasperis, A.; Conforti, M.; Baronio, F. & Wabnitz, S. (2007). Effects of nonlinear wave coupling: Accelerated solitons. Boomerons: From curiosity to nonlinear optics, *Eur. Phys. J. Special Topics*, Vol. 147, pp. 233-252

Degasperis, A. (2009). Multiscale expansion and integrability of dispersive wave equations. In: Mikhailov, A.. Integrability. *Lecture Notes in Physics*, Vol. 767, Springer, pp. 215-244

Degasperis, A. & Lombardo, S. (2009). Multicomponent integrable wave equations II. Soliton solutions, submitted to Journal of Physics A: Mathematical and Theoretical

Fournier, S.; Lopez-Martens, R.L.; Le Blanc, C.; Baubeau, E. & Salin, F. (1998). Solitonlike pulse shortening in a femtosecond parametric amplifier, *Opt. Lett.*, Vol. 23, pp. 627-629

Gale, G.M.; Cavallari, M.; Driscoll, T.J.; & Hache, F. (1995). Sub-20-fs tunable pulses in the visible from an 82-MHz optical parametric oscillator, *Opt. Lett.*, Vol. 20, pp. 1562-1564

Hasegawa, A. (1984). Generation of a train of soliton pulses by induced modulation instability in optical fibers *Opt. Lett.*, Vol. 9, pp. 288-290

Ibragimov, E.; and A. Struthers, A. (1996). Second-harmonic pulse compression in the soliton regime *Opt. Lett.*, Vol. 21, pp. 1582-1584

Ibragimov, E.; & Struthers, A. (1997). Three-wave soliton interaction of ultrashort pulses in quadratic media *J. Opt. Soc. Am B*, Vol. 14, pp.1472-1479

Ibragimov, E.; Struthers, A & Kaup, D.J. (1998). Soliton pulse compression in the theory of optical parametric amplification *Optics Comm.*, Vol. 32, pp. 101-107

Ibragimov, E.; Struthers, A; Kaup, D.J.; Khaydarov, J.D. & Singer K.D. (1999). Three-wave interaction solitons in optical parametric amplification *Phys. Rev. E*, Vol. 59, pp. 6122- 6137

Inoue, T.; Hiroishi, J.; Yagi, T.; & Mimura, Y. (2007). Generation of in–phase pulse train from optical beat signal *Opt. Lett*, Vol. 32, pp. 1596-1598

Kaup, D.J. (1976). The three-wave interactiona nondispersive phenomenon *Stud. Appl. Math.*, Vol. 55, pp. 9-44

Kaup, D.J.; Reiman, A.& Bers, A. (1979). Space-time evolution of nonlinear three-wave interactions. I. Interaction in a homofeneous medium *Rev. Mod. Phys.*, Vol. 51, pp. 275-309

Kaup, D.J. (1981). The solution of a general initial value problem for the full three dimensional three-wave resonant interaction *Physica D*, Vol. D3, pp. 374–395

Nozaki, K.; & Taniuti, T. (1973). Propagation of solitary pulses in interactions of plasma waves. II, *J. Phys. Soc. Japan*, Vol. 36, pp.591-595

Ohsawa, Y.; & Nozaki, K.(1974). Propagation of solitary pulses in interactions of plasma waves, *J. Phys. Soc. Japan*, Vol. 34, pp.796-800

Liu, Y.; Park, S.G.; & Weiner,A.M. (1996). Enhancement of narrow-band terahertz radiation from photoconducting antennas by optical pulse shaping, *Opt. Lett.*, Vol. 21, pp.1762- 1764

Longhi, S.; Marano, M.; Laporta, P.; Svelto, O.; Belmonte, M.; Agogliati, B.; Arcangeli, L.; Pruneri, V.; Zervas, M.N.; & Ibsen, M. (2000). 40-Ghz pulse-train generation at 1.5 um with a chirped fiber gratings as frequency multiplier, *Opt. Lett.*, Vol. 24, pp.1481- 1483

Petropoulos, P.; Ibsen, M.; Zervas, M.N.; & Richardson, D.J. (2000). Repetition frequency quadruplication through Fabry-Perot filtering, *Opt. Lett.*, Vol. 25, pp.521-523

Picozzi, A.; & Haelterman, M.(1998). Spontaneous formation of symbiotic solitary waves in a backward quasi-phase-matched parametric oscillator, *Opt. Lett.*, Vol. 23, pp.1808-1810

Pitois, S.; Fatome, J.; & Millot, G. (2002). Generation of a 160-Ghz transform limited pedestal free pulse train thorough multiwave mixing compression of a dual-frequency beat signal, *Opt. Lett.*, Vol. 27, pp.1729-1731

Stabinis, A.; Valiulis, G. & Ibragimov, E.A (1991). Effective sum frequency pulse compression in nonlinear crystals, *Optics Comm.*, Vol. 86, pp. 301-306

Taranenko, Y. N., & Kazovsky, L. G. (1992). Three-Wave Envelope Solitons: Can the Speed of Light in the Fiber be Controlled, *IEEE Phot. Tech. Lett.*, Vol. 4, pp. 494-497

Umstadter, D.; Esarey, E.; & Kim, J. (1994). Nonlinear plasma waves resonantly driven by optimized laser pulse trains, *Phys. Rev. Lett.*, Vol. 72, pp. 1224-1227

Wang, Y.; & Dragila, R. (1990). Efficient conversion of picosecond laser pulses into secondharmonic frequency using group-velocity dispersion, *Phys. Rev. A*, Vol. 41, pp.5645- 5649

Wang, Y.; & Luther-Davies, B. (1992). Frequency-doubling pulse compressor for picosecond high-power neodymium laser pulses, *Opt. Lett.*, Vol. 17, pp.1459-1461

Weiner, A.M.; Leaird, D.E., Wiederrecht, G.P.; & Nelson K.A. (2007). Femtosecond pulse sequences used for optical manipulation of molecular motion, *Science*, Vol. 247, pp.1317-1319

Yiannopoulos, K.; Vyrsokinos, K.; Kehayas, E.; Pleros, N.; Vlachos, K.; Avramopoulos, H.; & Guekos, G. (2003). Repetition frequency quadruplication through Fabry-Perot filtering, *IEEE Photon. Technol. Lett.*, Vol. 15, pp.1294-1296

Zakharov, V.E. & Manakov, S.V. (1973). Resonant interaction of wave packets in nonlinear media , *Sov. Phys. JETP Lett.*, Vol. 18, pp.243-245

Zakharov, V.E.; Manakov,S.V.; Novikov,S.P.; & Pitajevski (1980) *The Theory of Solitons: The Inverse Problem Method* Nauka.

Zakharov, V.E. (1991) *What is integrability?*, Springer Verlag.

Zhang, X.; Lytle, A.L.; Popmintchev, T.; Zhou, X.; Kapten, H.C.; Murnane, M.M.; & Cohen, O. (2007). Quasi-phase-matching and quantum-path control of high harmonic generation using counterpropagating light, *Nat. Phys.*, Vol. 3, pp.270-275

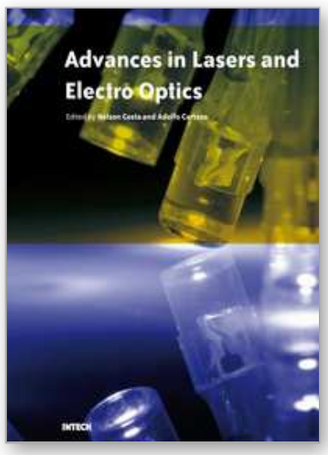

Advances in Lasers and Electro Optics

Edited by Nelson Costa and Adolfo Cartaxo

ISBN 978-953-307-088-9
Hard cover, 838 pages
Publisher InTech
Published online 01, April, 2010
Published in print edition April, 2010

Lasers and electro-optics is a field of research leading to constant breakthroughs. Indeed, tremendous advances have occurred in optical components and systems since the invention of laser in the late 50s, with applications in almost every imaginable field of science including control, astronomy, medicine, communications, measurements, etc. If we focus on lasers, for example, we find applications in quite different areas. We find lasers, for instance, in industry, emitting power level of several tens of kilowatts for welding and cutting; in medical applications, emitting power levels from few milliwatt to tens of Watt for various types of surgeries; and in optical fibre telecommunication systems, emitting power levels of the order of one milliwatt. This book is divided in four sections. The book presents several physical effects and properties of materials used in lasers and electro-optics in the first chapter and, in the three remaining chapters, applications of lasers and electro-optics in three different areas are presented.

InTech Europe
University Campus STeP Ri
Slavka Krautzeka 83/A
51000 Rijeka, Croatia
Phone: +385 (51) 770 447
Fax: +385 (51) 686 166
www.intechopen.com

InTech China
Unit 405, Office Block, Hotel Equatorial Shanghai
No.65, Yan An Road (West), Shanghai, 200040, China
中国上海市延安西路65号上海国际贵都大饭店办公楼405单元
Phone: +86-21-62489820
Fax: +86-21-62489821

IntechOpen